Journal of Nuclear Medicine, published on January 27, 2022 as doi:10.2967/jnumed.121.263309

Title: Evaluation of Data-Driven Rigid Motion Correction in Clinical Brain PET Imaging

Authors: Matthew G. Spangler-Bickell, PhD[1,2], Samuel A. Hurley, PhD[2], Ali Pirasteh, MD[2,3], Scott B. Perlman, MD[2], Timothy Deller[1], Alan B. McMillan, PhD[2,3]

Author affiliations: [1] PET/MR Engineering, GE Healthcare, Waukesha, WI, USA.

[2] Radiology, University of Wisconsin–Madison, WI, USA.

[3] Medical Physics, University of Wisconsin–Madison, WI, USA.

Corresponding author: MSB: matthew.spangler-bickell@ge.com

3200 N Grandview Blvd, Waukesha, WI, USA, 53188-1678

Tel: N/A

Fax: N/A

Disclaimers: MSB and TD are employees of GE Healthcare.

Funding information: Research reported in this publication was supported by the National Institute of Biomedical Imaging and Bioengineering (NIBIB) of the National Institutes of Health under award number R01EB026708.

Word count: 5235 words

Running title: Data-Driven Motion Correction Evaluation

Immediate Open Access: Creative Commons Attribution 4.0 International License (CC BY) allows users to share and adapt with attribution, excluding materials credited to previous publications.

License: https://creativecommons.org/licenses/by/4.0/.

Details: https://jnm.snmjournals.org/page/permissions.

Abstract

Head motion during brain PET imaging can cause significant degradation of the quality of the reconstructed image, leading to reduced diagnostic value and inaccurate quantitation. A fully data-driven motion correction approach was recently demonstrated to produce highly accurate motion estimates (< 1 mm) with high temporal resolution (≥ 1 Hz), which can then be used for a motion corrected reconstruction. This can be applied retrospectively with no impact on the clinical image acquisition protocol. We present a reader-based evaluation and an atlas-based quantitative analysis of this motion correction approach within a clinical cohort.

Methods: Clinical patient data were collected over 2019–2020 and processed retrospectively. Motion estimation was performed using image-based registration on reconstructions of ultra-short frames (0.6–1.8 s), after which fully motion corrected list-mode reconstructions were performed. Two readers graded the motion corrected and uncorrected reconstructions. An atlas-based quantitative analysis was performed. Paired Wilcoxon tests were used to test for significant differences in the reader scores and standard uptake values between the reconstructions. Levene's test was used to test whether motion correction had a greater impact on the quantitation in the presence of motion than when low motion was observed.

Results: 50 standard clinical ^{18}F-fluorodeoxyglucose brain PET data sets (age range 13–83 years, mean age ± standard deviation 59 ± 20 years, 27 women) from 3 scanners were collected. The reader study showed a significantly different, diagnostically relevant improvement by motion correction for cases where motion was present ($p = 0.02$) and no impact in low motion cases. 8% of all data sets improved from diagnostically "unacceptable" to "acceptable". The atlas-based analysis demonstrated a significant difference between the motion corrected and uncorrected reconstructions in cases of high motion for 7 of 8 ROIs ($p < 0.05$).

Conclusion: The proposed data-driven motion estimation and correction approach demonstrated a clinically significant impact on brain PET image reconstruction.

Keywords: PET; image reconstruction; data-driven motion correction; brain imaging

Introduction

As the spatial resolution of modern whole-body positron emission tomography (PET) scanners reaches 2-4 mm full-width at half-maximum (FWHM), together with improved sensitivity and time of flight (TOF) resolution, it is becoming increasingly likely that even small head motion may substantially degrade the reconstructed image. While patient motion with translations of up to 15 mm and rotations of up to 4^{o} are reported (*1*,*2*), smaller motions are quite common. Various motion tracking and correction techniques have been presented to account for head motion (*2*–*7*). These usually use an external tracking device (such as a camera) to track a marker attached to the head (*5*) or directly track the head (*6*). The motion estimates can then be used to perform frame-based reconstructions (*8*) or a full event-by-event motion corrected reconstruction (*9*,*10*). However, none of these motion correction approaches have been implemented into wide-spread standard clinical routine. This fact can be attributed to several reasons. Some patient motion can be partially managed through head restraints and discarding motion-corrupted portions of the data. To date, most motion tracking methods rely upon external hardware around the scanner (such as cameras) and/or attached to the patient (such as head markers), which complicate routine clinical protocols. Until recently there has not been a substantial effort from vendors to incorporate motion correction into their products and it has thus remained predominantly within the research setting.

Fully data-driven approaches to motion correction have been presented which do not require external hardware. These usually estimate when motion occurred so that the data can be suitably framed (*11*) or estimate the motion itself to be used in a motion corrected reconstruction (*12*–*15*). Due to typically low count rates in PET imaging and long reconstruction times, the temporal resolution used for such motion estimation is usually on the order of tens of seconds or longer. Such low temporal resolution may lead to residual intra-frame motion blurring and inaccurate motion estimates. Alternatively, when higher temporal resolutions are used (on the order of ~1 s) as in (*12*,*13*), the motion is estimated using centroid-of-distributions or inertial tensors calculations.

In this work we present an evaluation of a recently proposed data-driven motion estimation and correction approach (*16*,*17*). The motion is estimated using rigid image registration on reconstructed images of very short frames (0.6 – 1.8 s duration). The estimated motion is then used in a full event-by-event motion corrected list-mode reconstruction of the data including all PET corrections. The approach is completely data driven and can be applied retrospectively. An evaluation on a cohort of 50 standard clinical ^{18}F-fluorodeoxyglucose (^{18}F-FDG) brain PET data sets is presented, showing results of a reader study and an atlas-based quantitation analysis.

Materials and Methods

Data

Patient data were acquired at the Wisconsin Institutes for Medical Research at the University of Wisconsin–Madison, WI, USA, over 2019 and 2020, from a 4-ring Discovery MI (D-MI) PET/CT (20 cm axial field of view), a Discovery 710 (D710) PET/CT, and a SIGNA PET/MR (all from GE Healthcare, Chicago, IL, USA). All cases constituted routine clinical imaging studies for which an IRB-approved waiver of consent was obtained. Fifty consecutive ^{18}F-FDG brain PET data sets were collected retrospectively for this study, and none were rejected. Preliminary results from this study using these data sets were presented at the SNMMI 2021 conference (*18*); the current work presents a more thorough analytical and statistical analysis.

Motion estimation and image reconstruction

The data were processed in two steps before being analyzed. A flow diagram of the study is shown in Figure 1. First, ultra-fast reconstructions of very short frames (*16*) (0.6 – 1.8 s per frame, set automatically and adjusted at each frame to ensure a constant number of 500×10^3 true and scattered events per frame (*17*)) were performed for the entire scan duration, and image-based registration was then performed on these frames to estimate the motion. A rigid registration was performed using a least-squares metric and a gradient descent optimizer; further details are given in (*17*). The 6 degrees-

of-freedom (DOFs) of the motion were thus estimated directly at about 1 Hz, with an accuracy of < 1 mm (measured as the mean error in absolute displacement of a mesh of points moved by the estimated motion) (*17*). The reference frame for the image registrations was chosen to ensure that the PET reconstruction aligned with the attenuation map. In the case of PET/MR, the MR acquisitions for the attenuation map occur concurrently with the PET acquisition, thus the PET frames corresponding to data acquired during the MR attenuation correction pulse sequence were averaged to create the reference frame. For PET/CT, however, the CT acquisition occurs prior to the PET acquisition, thus, after estimating motion using the first PET frame as the reference, a single, automatic, cross-modality registration is performed using a mutual information metric to set this reference frame to align with the CT. The mean of all the short PET frames, after aligning them according to the estimated motion, was used for this registration. For 12 of the 29 PET/CT data sets, the automated cross-modality registration between the PET and the CT was suboptimal and manual intervention was required to ensure a good registration. This registration step will be made more robust in the future to ensure fully automated processing.

The data were categorized into four motion groups using a metric based upon the magnitude of the motion for each data set. Similarly to prior literature (*19*,*20*) we categorized the motion by moving points in image space and measuring their displacement. While others have used an average displacement, we were interested in the maximum extent of the motion, and thus two points at the extreme extent of the brain were sufficient. Two points located in image space at 70 mm anterior and 70 mm posterior to the brain center were chosen and moved according to the estimated motion parameters. The brain center relative to the scanner center was set at a typically observed value for each scanner: for the PET/MR at [left-right, anterior-posterior, superior-inferior] = [0, 40, 20] mm (the anterior-posterior offset was due to the head coil used), and for both PET/CTs at [0, 0, 20] mm. The median absolute displacement from the reference was calculated for each point. The larger of these two medians was used as a metric to classify the data sets into four motion groups:

Low: Median displacement less than 1 mm.

Offset: Median displacement less than 1 mm, but an initial displacement greater than 2 mm.

Medium: Median displacement between 1 mm and 2 mm.

High: Median displacement greater than 2 mm.

The Offset motion group captures those data sets with little motion during the PET acquisition but with a large offset between the attenuation map acquisition and the PET (this usually only applies to PET/CT scans). This group classification was chosen empirically based on our experience with many clinical data sets.

Following estimation of head motion a full reconstruction was performed with each event being corrected according to the estimated motion, as shown in Figure 1. A list-mode TOF-based block sequential regularization expectation maximization (BSREM) algorithm (*21*,*22*) was performed with a beta parameter of 50. A spatially-variant point-spread function (PSF) modelling is performed using a hybrid image-space / projection-space approach (*23*). For clarity the list-mode maximum likelihood expectation maximization (MLEM) with motion correction (*9*,*10*) is given here; subsets and a regularization term are added for the BSREM implementation:

$$\lambda_j^{n+1} = \frac{\lambda_j^n}{\bar{s}_j} \sum_m^M c_{i'_m j} \frac{1}{\sum_k c_{i'_m k} \lambda_k^n + \frac{S'_{i_m} + R_{i_m}}{a_{i'_m} e_{i_m} \sigma_{i_m}}},$$

$$\bar{s}_j = \sum_p^P w_p \sum_l^L c_{l'_p j} a_{l'_p} e_l \sigma_l ,$$

where λ_j^n is the image value at pixel j and iteration n, i_m is the line-of-response (LOR, the line joining a detecting crystal pair) i associated with list-mode event m, M is the total number of list-mode events, i'_m is the motion corrected LOR i for event m, c_{ij} is the system matrix, S'_i is the motion-aware scatter contribution along LOR i, R_i is the randoms contribution, a_i is the attenuation correction factor through

the patient attenuation map along LOR i, e_i is the attenuation correction factor through the attenuating material exterior to the patient along LOR i, σ_i is the scanner sensitivity factor (crystal efficiency and deadtime) for LOR i. The time-averaged sensitivity image $\bar{s}$ is calculated by moving the endpoints of each LOR (l, of which there are L in the scanner) by a particular set of motion parameters p, backprojecting the appropriate attenuation and sensitivity factors, and calculating the time-weighted (w_p) average across all the motion data, P. The attenuation factors a_i and e_i are handled separately since the patient is moving while the rest of the attenuating material is not, therefore the motion corrected LORs (i'_m) are used for the patient attenuation correction factors.

Additionally, a non-motion corrected list-mode reconstruction was performed for comparison.

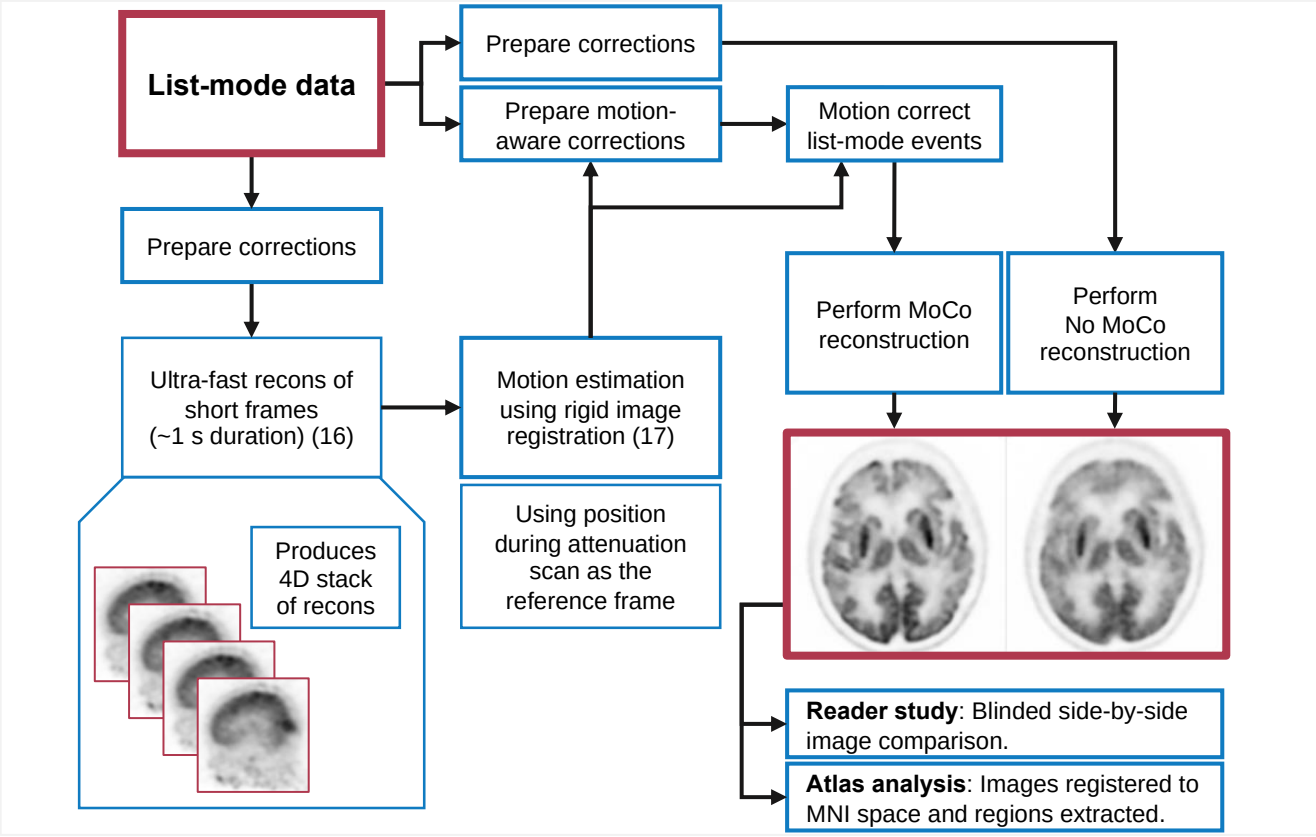

FIGURE 1: Flow diagram of the reconstruction process and analysis. MoCo: motion corrected. MNI: Montreal Neurosciences Institute.

Reader study

The motion corrected (MoCo) and non-motion corrected (No MoCo) reconstructions were randomized and read blinded by a nuclear medicine physician with 36 years of experience (author SP) and a dual-board certified nuclear medicine physician and radiologist with fellowship training in nuclear medicine and body MRI with 2 years of experience (author AP). Images were evaluated on a 5-point Likert scale for “image sharpness” and “diagnostic quality”, as specified in Table 1. The readers were not made aware of the motion groups of the data sets; these were used only during the analysis.

Quantitative analysis

An atlas-based analysis of the quantitative accuracy of the reconstructions was performed. The reconstructions were individually and non-rigidly registered to an aggregated FDG atlas in Montreal Neurosciences Institute-152 (MNI152) image space (*24*,*25*) using the Advanced Normalization Tools (ANTs) toolbox (*26*). Eight regions of interest (ROIs) were extracted and analyzed: frontal lobe, occipital lobe, temporal lobe, parietal lobe, cerebellum, left/right cerebral cortex, and whole cerebral cortex.

Statistical analysis

For the reader study, the inter-reader variability was tested using two metrics: as recommended by (*27*) the modified interrater agreement index (r_{wg}^{*}) was used to evaluate the 5-point Likert scores, and Cohen’s kappa (κ) (*28*) was used to evaluate the agreement of whether an image was diagnostically acceptable or not (i.e. having a Likert score of ≥ 3). These tests were conducted for both reader questions, and for the No MoCo and MoCo reconstructions.

Using the average Likert scores for the two readers, paired Wilcoxon tests were conducted to test for significant differences between the median scores of the MoCo and No MoCo reconstructions, at the two-sided $p < 0.05$ significance level, using the statistical toolbox in MATLAB (*29*). The false discovery rate (FDR) was corrected for using the Benjamini-Hochberg procedure with a rate (Q-value) of 10%.

For the atlas-based quantitative analysis, paired Wilcoxon tests for significant differences between the medians of the ROI SUV_{max} values in the MoCo and No MoCo reconstructions within each motion group were conducted at the two-sided $p < 0.05$ significance level, with FDR correction. Additionally, the relative differences between the SUV_{max} values of the MoCo and No MoCo reconstructions were calculated, and Levene's tests (*30*) were conducted to test whether the variance in these differences for each motion group was significantly different to the Low motion group in order to provide an indication that motion correction had made a quantitative difference in reconstructions when motion was present. A two-sided significance level of $p < 0.05$ was used and FDR correction was applied.

Results

Data Characteristics

A cohort of 50 standard clinical FDG brain data sets (age range 13 – 83 years, mean age ± standard deviation 59 ± 20 years, 27 women) was collected retrospectively from three scanners: D710 PET/CT (n = 18), D-MI PET/CT (n = 11), and SIGNA PET/MR (n = 21). The injected activity for the data sets from the three scanners was (mean ± standard deviation): D710 PET/CT: 390 ± 24 MBq (55 ± 4 min uptake time, 15 minutes duration, $4.6 \pm 1.1 \times 10^8$ counts), D-MI PET/CT: 400 ± 26 MBq (56 ± 5 min uptake time, 15 minutes duration, $8.9 \pm 2.3 \times 10^8$ counts), and SIGNA PET/MR: 450 ± 85 MBq (63 ± 13 min uptake time, 25 minutes duration, except 3 data sets with 11 – 15 minutes duration, $17.2 \pm 5.3 \times 10^8$ counts).

Motion estimation

The number of data sets in each motion group is shown in Table 2, and the distribution of the displacement metric is shown in Figure 2.

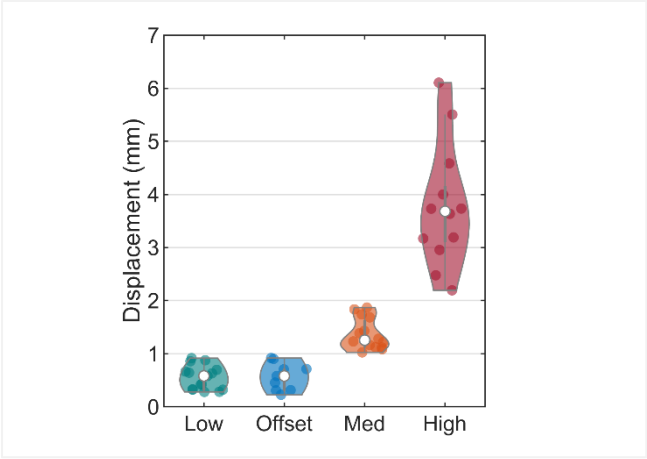

FIGURE 2: Violin plots (*31*) showing the distribution of the estimated motion for all data sets within the four motion groups. The width of the violins indicates the density of data points, and their length indicates the range of the data. The actual data points are scattered within the violins, with the white dot being the median.

Motion correction case studies

Three examples of reconstructions are shown in Figure 3 from the Low, Offset, and High motion groups.

The relative differences images shown were calculated as (MoCo – No MoCo)/MoCo × 100%.

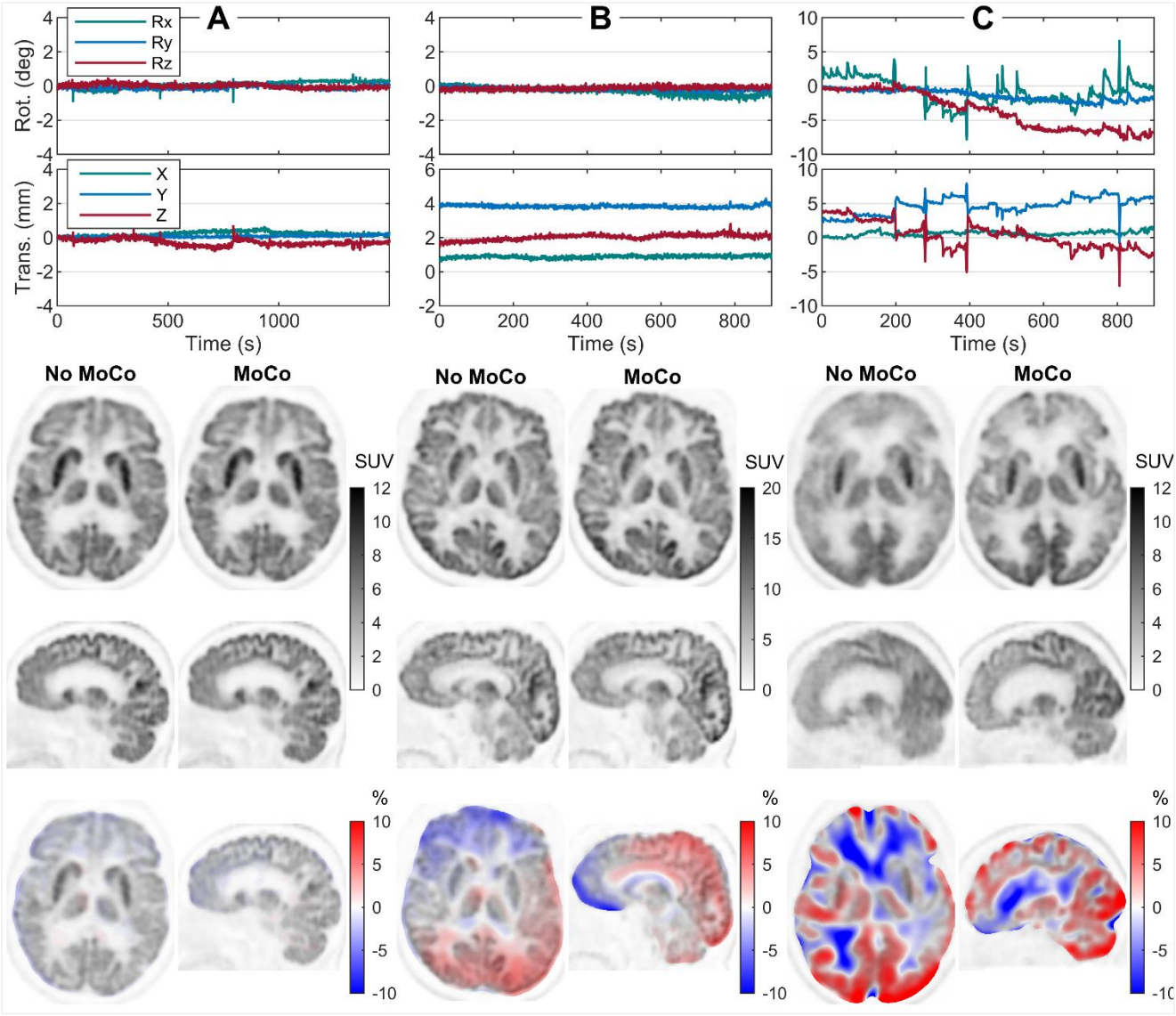

FIGURE 3: Example reconstructions for three case studies from the (A) Low, (B) Offset, and (C) High motion groups. All three are PET/CT data. The 6 DOFs of the motion data are plotted at the top. The smoothed relative differences between the images are shown at the bottom overlayed on the MoCo image. The Low motion case (A) demonstrates that when there is little motion the MoCo has a very small effect on the reconstruction. The Offset case (B) shows that while no obvious differences are visible between the images, the relative difference image shows a gradient due to the misalignment of the No MoCo image with the attenuation map. In the High motion case (C) much of the blurring due to motion visible in the No MoCo image has been removed in the MoCo image. Rot.: Rotation. Trans.: Translation.

Reader study

The results of the inter-reader variability analysis are shown in Table 3. The agreement between the readers was high according to all the tests. Notably, the agreement between the readers on whether

an image was diagnostically acceptable (κ) was higher (no disagreement) for the MoCo reconstructions than the No MoCo reconstructions (where there was one disagreement). The Likert scores for the two readers are shown in Figure 4 for the two questions. In 5 (10%) of the 50 data sets the diagnostic quality of the reconstruction improved with motion correction by ≥ 1 on the Likert scale. The No MoCo reconstructions for four (8%) data sets were rated as "not diagnostically acceptable" and for all of these the MoCo reconstructions were rated as "diagnostically acceptable." The results of the paired Wilcoxon tests on the reader scores are shown in Table 4.

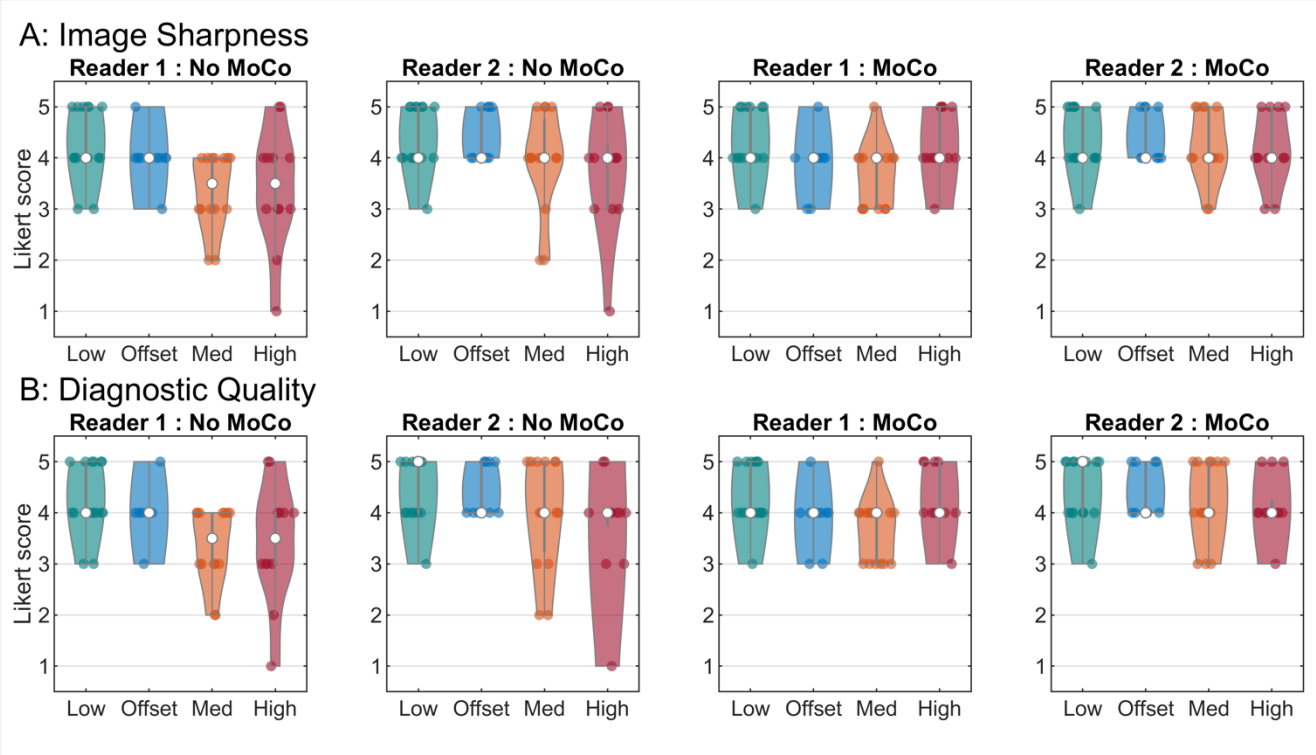

FIGURE 4: The Likert scores for the MoCo and No MoCo reconstructions for the two questions: (A) Image sharpness, and (B) Diagnostic quality. In the No MoCo cases the reader scores had more variation among the data sets in the higher motion groups, with some images being not diagnostically acceptable, while in the MoCo cases the scores were consistent across all motion groups.

Quantitative analysis

The relative differences in the ROI SUV_{max} values between the MoCo and No MoCo reconstructions are shown in Figure 5, calculated as $(S_M - S_N)/S_M \times 100\%$ where S_M and S_N refer to the SUV_{max} values

for the MoCo and No MoCo reconstructions, respectively. Table 5 presents the results of the statistical analysis.

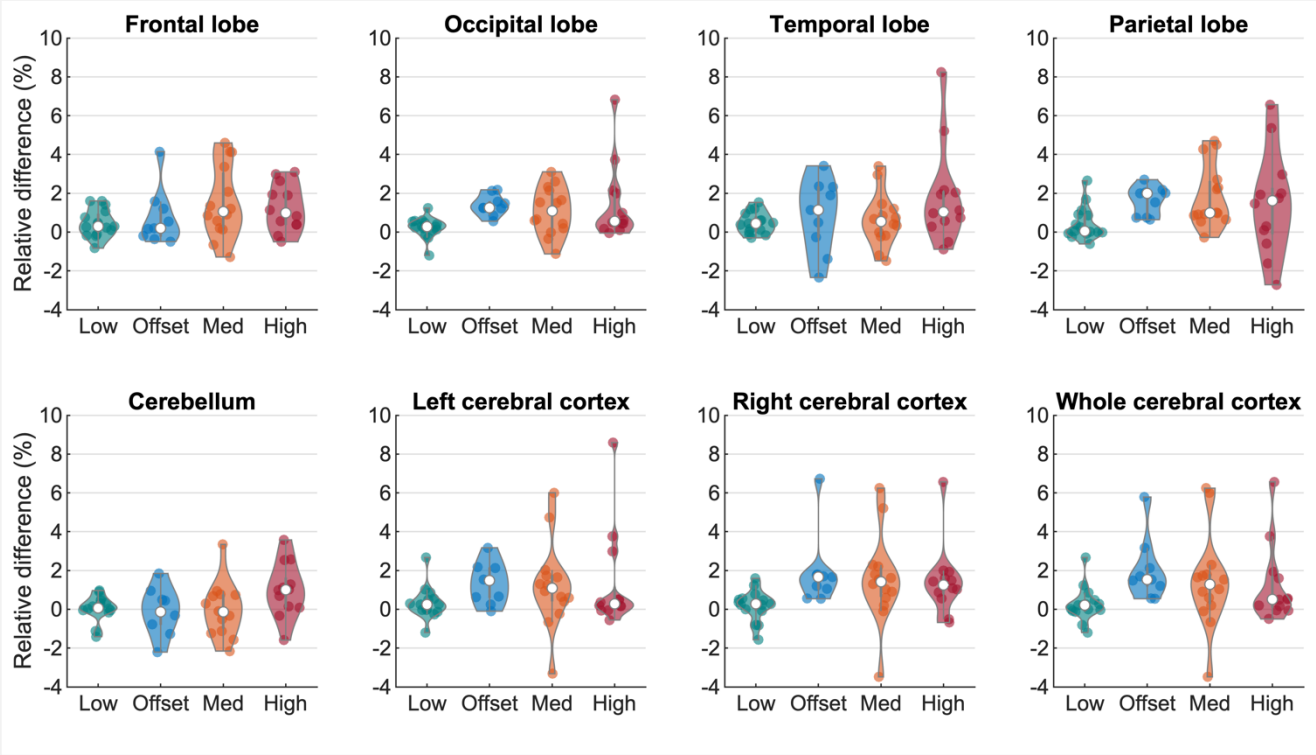

FIGURE 5: Relative differences between the SUV_{max} of the ROIs extracted from the MoCo and No MoCo reconstructions. The differences are larger in magnitude in the higher motion groups, as expected. Note that since the MoCo reconstruction ensures better alignment with the attenuation map, the SUV_{max} are expected to be more accurate in the MoCo reconstructions as compared to the No MoCo reconstructions, regardless of which is greater or lesser.

In Figure 5 it can be seen that the relative differences in SUV_{max} between the MoCo and No MoCo reconstructions were larger in the higher motion groups as compared to the Low motion group. In the High motion group the SUV_{max} of the parietal lobe in the MoCo reconstructions differed from those of the No MoCo reconstructions by 1.5 ± 2.7% (mean ± standard deviation) with a maximum of 6.6%, and in the temporal lobe the SUV_{max} differed by 1.8 ± 2.6% with a maximum of 8.2%. In all cases the SUV_{max} in the MoCo reconstruction are assumed to be more accurate, whether it is higher or lower than the No MoCo reconstruction, since the former ensures better alignment with the attenuation map and has reduced motion blurring. Table 5(a) demonstrates that in the High motion group the SUV_{max} values

between the MoCo and No MoCo reconstructions were significantly different in 7 out of 8 ROIs. Even in the Offset group where there was minimal motion during the PET acquisition the motion correction made a significant difference in 5 of 8 ROI SUV_{max} values, due to the improved alignment with the attenuation map. Levene's tests indicated that the variance in the relative differences between the MoCo and No MoCo reconstructions was higher for 7 of the 8 ROIs in the Medium and High motion groups, as compared to the Low motion group (Table 5(b)). A visualization of these variances can be seen in the extent of the plots in Figure 5, comparing the higher motion groups to the Low motion group. The results in Table 5 indicate that when there was high motion the MoCo significantly changed the reconstruction. The results of the reader study then confirm that the MoCo reconstructions were preferred.

Discussion

An evaluation of a fully data-driven motion estimation and correction technique for reconstruction of brain PET data sets has been presented. 50 standard clinical FDG brain PET data sets were processed retrospectively, acquired on one PET/MR and two PET/CT scanners. No additional motion tracking hardware was used during the scan, and there was no impact on the standard clinical routine. The motion estimation used a temporal resolution of ~1 s and detected motion of more than 1 mm in 70% (35/50) of the data sets and more than 2 mm in 24% (12/50) of cases, the latter of which usually resulted in visually obvious differences between the MoCo and no MoCo reconstructions. The blinded reader study showed that the MoCo reconstructions improved the diagnostic quality in 10% (5/50) of the data sets, and the improvement was significant in the High motion group ($p = 0.02$) and when considering all the data ($p = 0.003$). In 8% (4/50) of the data sets the image was improved from diagnostically "unacceptable" to "acceptable", which is a substantial portion of the cohort. The atlas-based quantitative analysis found significant differences ($p < 0.05$) in the SUV_{max} in 7 of the 8 ROIs in the Medium and High motion groups, and no significant differences in 5 of 8 ROIs in the Low motion group. The reader study confirmed that the image quality of the MoCo reconstructions was preferred

over the No MoCo reconstructions when motion was present and did not affect the scores when no motion was present, while the atlas-based analysis confirmed that motion correction does affect the quantitation of the reconstructions in the presence of motion.

Our study incorporated data from 3 scanners with very different geometries, with the axial field of view ranging from 157 mm to 250 mm, and all scanners benefitted from motion correction. The higher sensitivity and TOF resolution of modern scanners allows for shorter frame durations to be used for motion estimation, and hence improved temporal sampling. To achieve optimal temporal sampling, scanner specific optimization may be necessary (*17*). Motion estimation and reconstruction were performed in a research setting and took approximately 2 hours, which was ~30% longer than the no MoCo reconstruction of the same data set. Significant speed-up is expected with software optimization and dedicated hardware (e.g., GPUs) to ensure that the approach can be clinically feasible in future work.

This study has some limitations. We focused on ^{18}F-FDG as it is the most common clinically used radiotracer. However, assuming that accurate motion estimates can be obtained with other radiotracers, we expect that motion correction would have a similar effect on reconstructions of such data sets. Accurate motion estimation has been demonstrated previously with ^{18}F-florbetaben (FBB) using this approach (*17*). Optical motion tracking was not available for comparison, as the data were processed retrospectively, and this comparison was not the intention of this work. Note that this work has not included exams where the activity distribution of the radiotracer inside the brain may change substantially during the scan, for example an ^{15}O-H_2O brain perfusion study, since the reference frame used for registration would not be representative of the entire data set. While an approach for motion estimation in such cases would be more challenging and is outside of the scope of the current work, we believe that a data-driven solution is possible and is the topic of ongoing research. Lastly, while an evaluation of the image quality before and after motion correction was conducted, the diagnostic

implications of the motion corrected images was not fully investigated. Considering the promising nature of our current results, we plan to further investigate the clinical impact of the application.

Conclusions

We have presented an evaluation of a data-driven head motion correction technique for brain PET imaging. We have demonstrated that motion is prevalent amongst standard clinical data sets and that motion correction has a significant impact on the reconstructions, both qualitatively and quantitatively. The application of motion correction had no detrimental impact on image quality or quantification when no motion was present. Because motion is a known confounder of clinical brain PET, utilizing data-driven motion correction will likely have important implications for diagnostic and research studies where motion may occur. Given that the proposed solution relies entirely on retrospective reconstruction, it could be readily adopted into routine PET imaging procedures.

Disclosure

M. Spangler-Bickell and T. Deller are employees of GE Healthcare. Data for this study was controlled by M. Spangler-Bickell (while he was with UW–Madison in 2020), A. McMillan, and S. Hurley.

Key points

Question: How effective is the proposed data-driven head motion correction technique?

Pertinent findings:

- Motion was observed in 70% of the study cohort consisting of 50 consecutively acquired data sets.
- A reader study showed that all data sets which were deemed diagnostically “unacceptable” without motion correction (8%, 4/50) were then diagnostically “acceptable” with motion correction, with a significant improvement in cases of high motion.
- An 8 ROI atlas-based quantitative analysis concluded that motion correction had a significant impact on SUV_{max} (up to 9%) in 65% of the ROIs.

Implications for patient care: Patient motion would no longer be a concern for FDG PET brain imaging when using this technology; patients can be scanned regardless of motion risk and any motion will be corrected.

References

1. Bloomfield PM, Spinks TJ, Reed J, et al. The design and implementation of a motion correction scheme for neurological PET. *Phys Med Biol*. 2003;48:959-978.

2. Lopresti BJ, Russo A, Jones WF, et al. Implementation and performance of an optical motion tracking system for high resolution brain PET imaging. *IEEE Trans Nucl Sci*. 1999;46:2059-2067.

3. Daube-Witherspoon M, Yan Y, Green M, Carson R, Kempner K, Herscovitch P. Correction for motion distortion in PET by dynamic monitoring of patient position. *J Nucl Med*. 1990;31:816.

4. Fulton RR, Meikle SR, Eberl S, Pfeiffer J, Constable CJ, Fulham MJ. Correction for head movements in positron emission tomography using an optical motion-tracking system. *IEEE Trans Nucl Sci*. 2002;49:116-123.

5. Spangler-Bickell MG, Khalighi MM, Hoo C, et al. Rigid Motion Correction for Brain PET/MR Imaging Using Optical Tracking. *IEEE Trans Radiat Plasma Med Sci*. 2019;3:498-503.

6. Kyme AZ, Aksoy M, Henry DL, Bammer R, Maclaren J. Marker-free optical stereo motion tracking for in-bore MRI and PET-MRI application. *Med Phys*. 2020;47:3321-3331.

7. Kyme AZ, Fulton RR. Motion estimation and correction in SPECT, PET and CT. *Phys Med Biol*. 2021;66.

8. Picard Y, Thompson CJ. Motion correction of PET images using multiple acquisition frames. *IEEE Trans Med Imaging*. 1997;16:137-144.

9. Carson RE, Barker WC, Liow JS, Johnson CA. Design of a Motion-compensation OSEM List-mode Algorithm for resolution-recovery Reconstruction for the HRRT. *IEEE Nucl Sci Symp Conf Rec*. 2003;5:3281-3285.

10. Rahmim A, Bloomfield P, Houle S, et al. Motion compensation in histogram-mode and list-mode EM reconstructions: Beyond the event-driven approach. *IEEE Trans Nucl Sci*. 2004;51:2588-2596.

11. Schleyer PJ, Dunn JT, Reeves S, Brownings S, Marsden PK, Thielemans K. Detecting and estimating head motion in brain PET acquisitions using raw time-of-flight PET data. *Phys Med Biol*. 2015;60:6441-58.

12. Feng T, Yang D, Zhu W, Dong Y, Li H. Real-time data-driven rigid motion detection and correction for brain scan with listmode PET. *IEEE Nucl Sci Symp Med Imaging Conf*. 2016.

13. Rezaei A, Spangler-Bickell M, Schramm G, Van Laere K, Nuyts J, Defrise M. Rigid motion tracking using moments of inertia in TOF-PET brain studies. *Phys Med Biol*. 2021;66:0-13.

14. Jin X, Mulnix T, Gallezot JD, Carson RE. Evaluation of motion correction methods in human brain PET imaging-A simulation study based on human motion data. *Med Phys*. 2013;40:1-12.

15. Mukherjee JM, Lindsay C, Mukherjee A, et al. Improved frame-based estimation of head motion in PET brain imaging. *Med Phys*. 2016;43:2443-2454.

16. Spangler-Bickell MG, Deller TW, Bettinardi V, Jansen F. Ultra-Fast List-Mode Reconstruction of Short PET Frames and Example Applications. *J Nucl Med*. 2021;62:287-292.

17. Spangler-Bickell MG, Hurley SA, Deller TW, et al. Optimizing the frame duration for data-driven rigid motion estimation in brain PET imaging. *Med Phys*. 2021;48:3031-3041.

18. Spangler-Bickell M, Hurley S, Pirasteh A, Perlman S, Deller T, McMillan A. Clinical Evaluation of Data-Driven Motion Corrected Reconstruction for PET Brain Imaging. *J Nucl Med*. 2021;62 (suppl 1):59.

19. Tisdall MD, Hess AT, Reuter M, Meintjes EM, Fischl B, Van Der Kouwe AJW. Volumetric navigators for prospective motion correction and selective reacquisition in neuroanatomical MRI. *Magn Reson Med*. 2012;68:389-399.

20. Jenkinson M. Measuring Transformation Error by RMS Deviation [Internet]. Oxford Centre for Functional Magnetic Resonance Imaging of the Brain (FMRIB) Technical Report TR99MJ1. http://www.fmrib.ox.ac.uk/analysis/techrep/tr99mj1/tr99mj1/index.html.

21. Ahn S, Fessler JA. Globally convergent image reconstruction for emission tomography using

relaxed ordered subsets algorithms. *IEEE Trans Med Imaging*. 2003;22:613-626.

22. Spangler-Bickell MG, Deller T, Jansen F. Accelerated Regularised List-Mode PET Reconstruction Using Subset Relaxation. *IEEE Nucl Sci Symp Med Imaging Conf*. 2019.

23. Deller TW, Ahn S, Jansen FP, et al. Implementation and image quality benefit of a hybrid-space PET point spread function. *IEEE Nucl Sci Symp Med Imaging Conf*. 2021.

24. Darkner S. FDG-PET template MNI152 1mm. 2013. Dataset.

25. Harvard-Oxford cortical and subcortical structural atlases [Internet]. https://identifiers.org/neurovault.collection:262.

26. Advanced Normalization Tools [Intenet]. http://stnava.github.io/ANTs/.

27. O'Neill TA. An overview of interrater agreement on likert scales for researchers and practitioners. *Front Psychol*. 2017;8:777.

28. Cohen J. A Coefficient of Agreement for Nominal Scales. *Educ Psychol Meas*. 1960;20:37-46.

29. MATLAB. MATLAB (R2020a). Natick, Massachusetts: The MathWorks Inc. https://www.mathworks.com/.

30. Levene H. Robust tests for equality of variances. *Contrib to Probab Stat Essays Honor Harold Hotell*. 1961:279-292.

31. Bechtold B. Violin Plots for Matlab, Github Project [Internet]. https://github.com/bastibe/Violinplot-Matlab.

TABLE 1: Likert-scale scoring for image evaluation.

Score	Criteria	Diagnostic Acceptability
1	Very poor	Non-diagnostic
2	Poor	Non-diagnostic
3	Acceptable	Diagnostic
4	Good	Diagnostic
5	Excellent	Diagnostic

TABLE 2: Distribution of data sets amongst the defined motion groups.

Group	All scanners	D710 PET/CT	D-MI PET/CT	SIGNA PET/MR
Low	15 (30%)	4	1	10
Offset	9 (18%)	4	5	0
Medium	14 (28%)	6	4	4
High	12 (24%)	4	1	7

TABLE 3: The results of the inter-reader variability analysis. The agreement was high in all cases.

	No MoCo		MoCo	
	r_{wg}^{*}	κ	r_{wg}^{*}	κ
Image Sharpness	0.98	0.85	0.98	1
Diagnostic Quality	0.98	0.85	0.98	1

TABLE 4: The p-values of the paired Wilcoxon tests between the MoCo and No MoCo reconstructions, according to the reader Likert scores. “All” indicates all motion groups considered together. An * indicates a significant difference ($p < 0.05$, FDR corrected).

Motion Group	Low	Offset	Medium	High	All
Image Sharpness	>0.99	>0.99	0.06	0.02*	0.003*
Diagnostic Quality	>0.99	>0.99	0.13	0.02*	0.003*

TABLE 5: (a) Results from the paired Wilcoxon tests on the ROI SUV_{max} of the MoCo and No MoCo images. (b) Results of the Levene's tests on the variance of the ROI SUV_{max} relative difference values. An * indicates a significant difference ($p < 0.05$, FDR corrected).

	(a) Wilcoxon test on SUV_{max}				(b) Levene's test on relative difference of SUV_{max}		
	Low	**Offset**	**Med**	**High**	**Offset**	**Med**	**High**
Frontal lobe	0.03*	0.25	0.009*	0.007*	0.10	0.002*	0.02*
Occipital lobe	0.03*	0.004*	0.009*	0.001*	0.73	0.001*	0.005*
Temporal lobe	0.007*	0.16	0.10	0.007*	0.001*	0.04*	0.01*
Parietal lobe	0.11	0.004*	<0.001*	0.08	0.89	0.01*	0.009*
Cerebellum	0.39	>0.99	0.71	0.03*	0.05	0.04*	0.04*
Left cerebral cortex	0.09	0.008*	0.02*	0.03*	0.20	0.0499*	0.01*
Right cerebral cortex	0.21	0.004*	0.01*	0.009*	0.24	0.07	0.24
Whole cerebral cortex	0.21	0.004*	0.03*	0.02*	0.13	0.04*	0.03*

Graphical Abstract

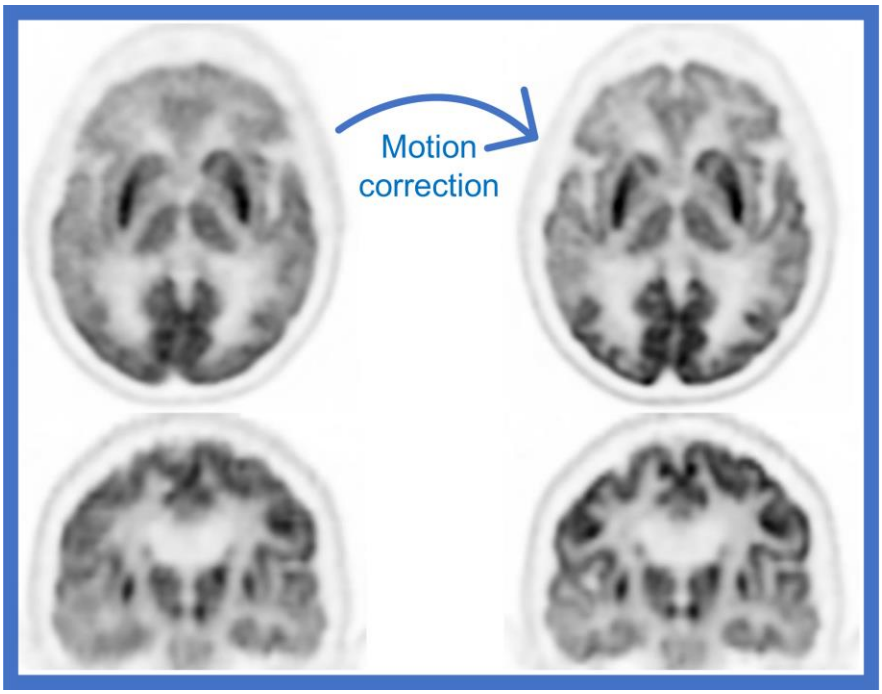

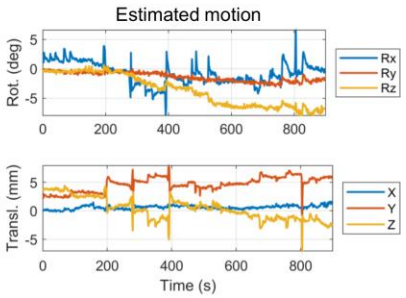

Data-driven motion correction using ~1 s frames with <1 mm accuracy.

The system spatial resolution is recovered for any head motion.

There is no impact on clinical routine or data acquisition.